

## Phonon Dispersion Relations for Caesium Thiocyanate

M. A. Irving,<sup>A</sup> M. M. Elcombe<sup>B</sup> and T. F. Smith<sup>A</sup>

<sup>A</sup> Department of Physics, Monash University, Clayton, Vic. 3168.

<sup>B</sup> Australian Atomic Energy Commission Research Establishment,  
Lucas Heights Research Laboratories, Private Mailbag, Sutherland, N.S.W. 2232.

### Abstract

Room temperature phonon dispersion relations for frequencies below 2 THz have been measured, along the three orthorhombic axes and selected diagonal directions by neutron inelastic scattering, for caesium thiocyanate. These curves, which represent 13 acoustic modes and 11 optic modes of vibration, do not agree with the dispersion behaviour calculated from the rigid-ion model developed by Ti and Ra to describe their Raman scattering observations.

### 1. Introduction

Caesium thiocyanate is a member of a class of ionic crystals consisting of spherical cations and rod-shaped anions. In general, the lowest temperature phase of these materials is orthorhombic. Transformations to phases of higher symmetry occur with increasing temperature, the highest temperature phase having a cubic structure. To achieve a symmetry higher than orthorhombic the linear thiocyanate anions must become orientationally disordered. For most of these materials the transformation to the final cubic phase takes place through several intermediate phases, but caesium thiocyanate transforms directly to a cubic structure from the room temperature orthorhombic phase. The alkali cyanides are the most extensively investigated compounds belonging to this class. By comparison the alkali thiocyanates, KSCN, CsSCN and RbSCN, have received little attention.

The crystal structure (Manolatos *et al.* 1973), optical spectra (Ti *et al.* 1977) and elastic constants (Irving *et al.* 1983), all at room temperature, have been reported for CsSCN. Differential thermal analysis (Manolatos *et al.* 1973; Klement 1976) has revealed the existence of a phase transition at 198°C. An X-ray structural investigation (Manolatos *et al.* 1973) established that the transition involved the disordering of the thiocyanate ions.

Lattice dynamical calculations based upon a rigid-ion model have been made for both potassium and caesium thiocyanate (Ra *et al.* 1978; Ra and Ra 1980*a*, 1980*b*). The model describes the interatomic forces in terms of a Coulombic interaction between the formal charges on the ions, and a short range Buckingham-type potential between nearest neighbours. The model parameters were determined from the conditions for static equilibrium of the lattice, and its stability with respect to variations of the unit cell parameters. The equilibrium conditions for caesium thiocyanate

alone are insufficient to fully determine values for the potential parameter set. Therefore, Ti and Ra found it necessary to use the equilibrium conditions for both caesium and potassium thiocyanate, assuming similar potential parameters for the interaction between thiocyanate ions, and differing metal to thiocyanate ion interactions. The short range potential is therefore a composite for the two materials.

To date, the experimental test of the model has been limited to the zone centre optic modes (Ra *et al.* 1978) and the initial slopes of the acoustic dispersion relations (Irving *et al.* 1983). In the former case the average absolute error between the calculated room temperature zone centre optic modes and the available optical spectra was 18%. In the latter case, the agreement between the calculated and measured acoustic velocities was generally quite reasonable, although there were some serious discrepancies. The present investigation provides the first experimental comparison between the calculated and measured phonon dispersion curves for an alkali thiocyanate and therefore represents the most stringent test of the model.

The complexity that is introduced into the lattice dynamics by the rotational freedom of the thiocyanate ion is the basic motivation for studying this particular compound. This investigation is part of a wider program to investigate the alkali thiocyanates with particular emphasis on the rotational modes of vibration, their relevance to the mechanism of the phase transition, and their interaction with acoustic modes of vibration. While this room temperature investigation does not directly address the problem of the phase transition, it is a starting point towards a better theoretical description of the lattice dynamics, and further measurements at higher temperatures.

## 2. Experimental

The room temperature structure of caesium thiocyanate is orthorhombic with space group *Pnma*, and lattice parameters  $a = 7.978$ ,  $b = 6.332$  and  $c = 8.332$  Å (Manolatos *et al.* 1973). Single crystals were grown from water solution by evaporation. The habit of the crystal is such that the growth is predominantly in the plane normal to the [001] direction. The crystal used in the present investigation was a flat disc 3.1 cm in diameter and 0.8 cm thick, substantially visually clear, and had a measured mosaic spread of less than 0.5° FWHM.

The phonon dispersion relations were mapped out using the 10H triple axis neutron spectrometer on the HIFAR reactor at the Australian Atomic Energy Commission Lucas Heights facility. This instrument is fully computer controlled and is in the 'W' scattering configuration. Incident wavelength selection was determined by Bragg reflection from the (111) planes of a single crystal of copper. Scattered wavelength selection was set by the (0004) reflection from a pyrolytic graphite crystal. The collimation before the sample was 0.7° FWHM and 1.3° FWHM before the analyser. The detector had an acceptance angle of 3°.

To resolve the phonon resonances it was necessary to use scattering angles greater than 45° from the monochromator. The majority of measurements were made using the 'constant Q' method with a fixed scattered neutron wavevector of 2.6 Å<sup>-1</sup>. For this wavevector, the energy resolution, as determined from a 'constant Q' scan using the elastic incoherent scatterer vanadium, was 0.16 THz. The calibration of the instrument and the alignment of the sample were such that the energy mismatch

between analyser and monochromator was at most 0.01 THz, and the error in the phonon  $q$  was  $\pm 0.05\%$ .

Measurements were made along each of the orthorhombic axes and selected diagonal directions. This required three settings of the crystal corresponding to each of the orthorhombic directions being mounted normal to the scattering plane. Counting times for the optical modes were long with some resonances taking 24 hours per peak. This forced the investigation to be limited to those modes below 2 THz. The largest scattering vector available at zero energy transfer was  $4.4 \text{ \AA}^{-1}$ .

There are four formula units in the primitive unit cell producing a total of 48 degrees of freedom, of which 32 correspond to rigid-ion translations and rotations. The dispersion relations therefore consist of 48 branches, which can be divided into 32 external lattice modes and 16 internal modes of the thiocyanate ion. At the zone centre ( $q = 0$ ) the external modes of the lattice can be decomposed into eight symmetry species labelled by their irreducible representations  $A_g$ ,  $B_{1g}$ ,  $B_{2g}$ ,  $B_{3g}$ ,  $A_u$ ,  $B_{1u}$ ,  $B_{2u}$  and  $B_{3u}$  (Ti *et al.* 1977). The numbers of phonon branches corresponding to each species are 8, 4, 8, 4, 4, 8, 4 and 8 respectively. The symmetric or 'gerade' representations  $A_g$ ,  $B_{1g}$ ,  $B_{2g}$  and  $B_{3g}$  are Raman active while the antisymmetric or 'ungerade' representations  $A_u$ ,  $B_{1u}$ ,  $B_{2u}$  and  $B_{3u}$  are infrared active. The arrangement of atoms within the unit cell is discussed in Section 4. All the atoms lie on mirror planes normal to  $[010]$ . The representations can be divided into those which only involve motions normal to the mirror planes,  $A_u$ ,  $B_{3g}$ ,  $B_{1g}$  and  $B_{2u}$ , and those which only have motions in the mirror planes,  $A_g$ ,  $B_{3u}$ ,  $B_{1u}$  and  $B_{2g}$ .

The dynamical structure factors for the various phonon branches were calculated from eigenvectors produced by the rigid-ion model of Ti and Ra (S. S. Ti, personal communication). These were initially used in an attempt to select the best position in the scattering plane to measure a particular branch, but with disappointing results. Consequently a survey of the intensities of Bragg reflections in the scattering plane was made and this was used as a guide to the best locations to observe the acoustic modes. The optic phonons were found by a systematic search of reciprocal space with due allowance for the symmetry of the crystal and the resolution 'focusing' of the triple axis. All accessible reciprocal lattice points within one quadrant of the scattering plane in reciprocal space, and several points in adjacent quadrants, were examined.

The possibility of extraneous resonances due to  $\frac{1}{2}\lambda$  contamination was catered for by using a computer program to predict their occurrence. Suspicious resonances were checked by repeating the measurements with slightly different scattered neutron wavelengths. There is also substantial self-consistency in the results which is not obvious in their final presentation. Many phonon branches were detected at several points in reciprocal space, and sometimes for more than one orientation of the crystal. In each case the best resonance was used to determine the energy.

### 3. Results

Three typical phonon resonances are shown in Fig. 1. The curves represent the least-squares function fits to the data points from which the energy centre was obtained. The majority of the resonances were fitted with a simple gaussian function and a linear background. This procedure was not possible in some cases because of overlapping resonances. In these cases the peak maxima were taken as the energy

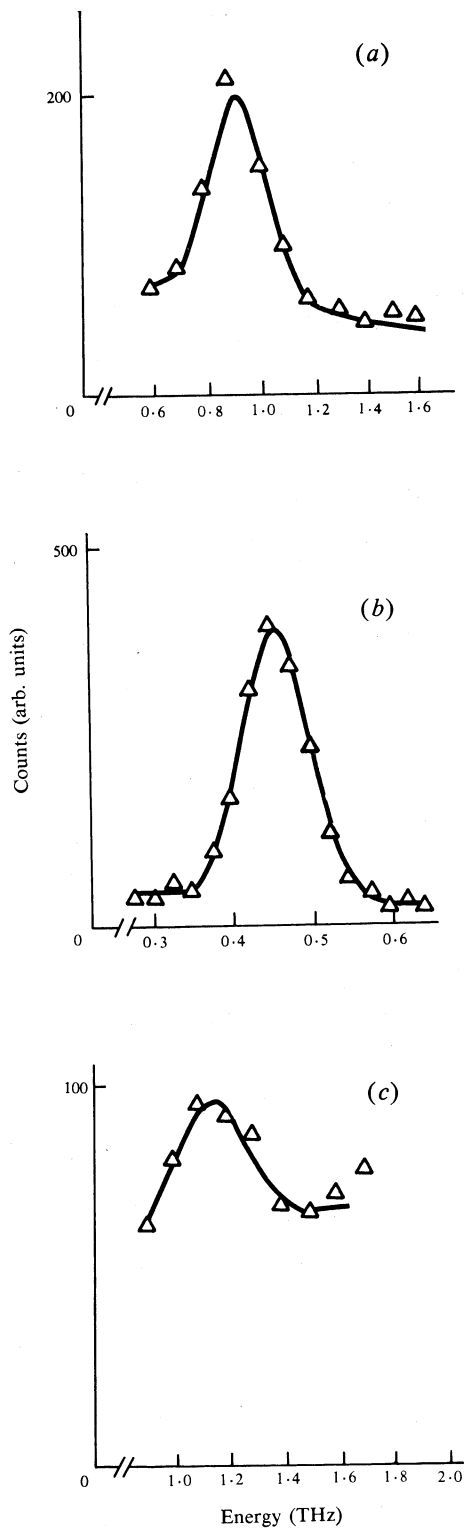


**Fig. 1.** Phonon resonances fitted by Gaussians and linear backgrounds: (a) optic mode,  $q = 0$ ; (b) transverse mode,  $q = [0.35\ 0\ 0]$  [0 1 0] polarization; (c) longitudinal mode,  $q = [0.5\ 0\ 0]$ .

Table 1. Collected phonons along the [100] direction

Phonon	$Q$	$q$	Energy (THz)
LA [100]	(5·143 0 -2)	[0·143 0 0]	0·500 (const. $E$ )
		$q \pm 0\cdot003$	
	(5·2 0 -2)	[0·2 0 0]	0·625 $\pm$ 0·015
	(5·25 0 -1)	[0·25 0 0]	0·767 $\pm$ 0·009
	(5·25 0 -2)	[0·25 0 0]	0·772 $\pm$ 0·021
	(5·296 0 -2)	[0·296 0 0]	0·900 (const. $E$ )
		$q \pm 0\cdot006$	
	(5·35 0 -2)	[0·35 0 0]	1·054 $\pm$ 0·034
	(5·4 0 -2)	[0·4 0 0]	1·277 $\pm$ 0·042
	(5·5 0 -2)	[0·5 0 0]	1·338 $\pm$ 0·043
TA [100]/[010]	(-0·15 4 0)	[0·15 0 0]	0·222 $\pm$ 0·010
	(-0·2 4 0)	[0·2 0 0]	0·271 $\pm$ 0·009
	(-0·25 4 0)	[0·25 0 0]	0·333 $\pm$ 0·009
	(-0·3 4 0)	[0·3 0 0]	0·392 $\pm$ 0·010
	(-0·35 4 0)	[0·35 0 0]	0·457 $\pm$ 0·010
	(-0·4 4 0)	[0·4 0 0]	0·518 $\pm$ 0·010
	(-0·45 4 0)	[0·45 0 0]	0·579 $\pm$ 0·010
	(-0·5 4 0)	[0·5 0 0]	0·640 $\pm$ 0·011
TA [100]/[001]	(-2·15 0 5)	[0·15 0 0]	0·291 $\pm$ 0·009
	(-2·2 0 5)	[0·2 0 0]	0·391 $\pm$ 0·009
	(-2·25 0 5)	[0·25 0 0]	0·493 $\pm$ 0·009
	(-2·3 0 5)	[0·3 0 0]	0·587 $\pm$ 0·009
	(-2·35 0 5)	[0·35 0 0]	0·678 $\pm$ 0·010
	(-2·4 0 5)	[0·4 0 0]	0·773 $\pm$ 0·009
	(-2·45 0 5)	[0·45 0 0]	0·854 $\pm$ 0·014
	(-2·5 0 5)	[0·5 0 0]	0·920 $\pm$ 0·009
Optic 7	(-0·9 4 0)	[0·1 0 0]	0·90 $\pm$ 0·10
	(-0·8 4 0)	[0·2 0 0]	0·90 $\pm$ 0·10
	(-0·7 4 0)	[0·3 0 0]	0·866 $\pm$ 0·016
	(5·3 0 -2)	[0·3 0 0]	0·89 $\pm$ 0·015
	(1·35 4 0)	[0·35 0 0]	0·834 $\pm$ 0·021
	(1·4 4 0)	[0·4 0 0]	0·770 $\pm$ 0·016
	(-0·6 4 0)	[0·4 0 0]	0·763 $\pm$ 0·011
Optic 8	(-0·1 0 5)	[0·1 0 0]	1·668 $\pm$ 0·033
	(-0·2 0 5)	[0·2 0 0]	1·640 $\pm$ 0·033
	(-2·7 0 5)	[0·3 0 0]	1·294 $\pm$ 0·032
	(-2·6 0 5)	[0·4 0 0]	1·059 $\pm$ 0·013
Optic 9	(0·9 4 0)	[0·1 0 0]	1·176 $\pm$ 0·027
	(1·1 4 0)	[0·1 0 0]	1·165 $\pm$ 0·020
	(1·15 4 0)	[0·15 0 0]	1·140 $\pm$ 0·027
	(-1·2 4 0)	[0·2 0 0]	1·172 $\pm$ 0·021
	(-1·3 4 0)	[0·3 0 0]	1·10 $\pm$ 0·1
	(1·35 4 0)	[0·35 0 0]	1·20 $\pm$ 0·1
	(1·4 4 0)	[0·4 0 0]	1·2 $\pm$ 0·1
	(1·5 4 0)	[0·5 0 0]	1·212 $\pm$ 0·046
Optic 10	(0·1 0 5)	[0·1 0 0]	1·814 $\pm$ 0·035
	(0·2 0 5)	[0·2 0 0]	1·748 $\pm$ 0·098
	(0·3 0 5)	[0·3 0 0]	1·802 $\pm$ 0·055
	(0·4 0 5)	[0·4 0 0]	1·626 $\pm$ 0·058
	(0·5 0 5)	[0·5 0 0]	1·485 $\pm$ 0·039

Table 2. Collected phonons along the [0 1 0] direction

Phonon	$Q$	$q$	Energy (THz)
LA [0 1 0]	(0 4.15 0)	[0 0.15 0]	0.607 ± 0.021
	(0 4.175 0)	[0 0.175 0]	0.689 ± 0.022
	(0 4.2 0)	[0 0.2 0]	0.765 ± 0.021
	(0 4.25 0)	[0 0.25 0]	0.866 ± 0.018
	(0 4.3 0)	[0 0.3 0]	0.875 ± 0.022
	(0 4.35 0)	[0 0.35 0]	0.905 ± 0.015
	(0 4.40 0)	[0 0.4 0]	0.858 ± 0.080
	(0 3.55 0)	[0 0.45 0]	0.795 ± 0.011
	(0 3.5 0)	[0 0.5 0]	0.750 ± 0.017
TA [0 1 0]/[1 0 0]	(2 2.15 0)	[0 0.15 0]	0.246 ± 0.009
	(2 2.2 0)	[0 0.2 0]	0.340 ± 0.012
	(2 2.25 0)	[0 0.25 0]	0.400 ± 0.011
	(2 2.3 0)	[0 0.3 0]	0.474 ± 0.013
	(2 2.35 0)	[0 0.35 0]	0.537 ± 0.015
	(2 2.4 0)	[0 0.4 0]	0.637 ± 0.014
	(2 2.5 0)	[0 0.5 0]	0.759 ± 0.008
TA [0 1 0]/[0 0 1]	(0 2.15 2)	[0 0.15 0]	0.223 ± 0.011
	(0 2.2 2)	[0 0.2 0]	0.288 ± 0.011
	(0 2.25 2)	[0 0.25 0]	0.364 ± 0.013
	(0 2.3 2)	[0 0.3 0]	0.435 ± 0.012
	(0 2.35 2)	[0 0.35 0]	0.518 ± 0.011
	(0 2.4 2)	[0 0.4 0]	0.590 ± 0.012
	(0 2.45 2)	[0 0.45 0]	0.662 ± 0.014
	(0 2.5 2)	[0 0.5 0]	0.741 ± 0.014
Optic 2	(0 4.1 1)	[0 0.1 0]	0.965 ± 0.024
	(0 4.15 1)	[0 0.15 0]	0.952 ± 0.028
	(0 4.175 1)	[0 0.175 0]	0.965 ± 0.024
	(0 4.2 1)	[0 0.2 0]	1.096 ± 0.010
	(0 4.2 0)	[0 0.2 0]	1.144 ± 0.029
	(0 4.25 0)	[0 0.25 0]	1.211 ± 0.013
	(0 4.3 0)	[0 0.3 0]	1.35 ± 0.1
	(0 4.4 0)	[0 0.4 0]	1.686 ± 0.081
	(0 4.5 0)	[0 0.5 0]	1.80 ± 0.1
	Optic 5	(0 3.1 1)	[0 0.1 0]
(1 4.1 0)		[0 0.1 0]	1.194 ± 0.030
(1 3.9 0)		[0 0.1 0]	1.199 ± 0.031
(0 3.15 1)		[0 0.15 0]	1.186 ± 0.015
(1 3.8 0)		[0 0.2 0]	1.278 ± 0.037
(0 3.75 -2)		[0 0.25 0]	1.40 ± 0.1
(1 3.7 0)		[0 0.3 0]	1.40 ± 0.1
(0 3.65 -2)		[0 0.35 0]	1.423 ± 0.030
(0 3.55 -2)		[0 0.45 0]	1.531 ± 0.028
Optic 4	(0 0.1 5)	[0 0.1 0]	1.776 ± 0.045
	(0 0.2 5)	[0 0.2 0]	1.72 ± 0.1
	(0 -0.3 5)	[0 0.3 0]	1.811 ± 0.049
	(0 -0.4 5)	[0 0.4 0]	1.65 ± 0.12
	(0 -0.5 5)	[0 0.5 0]	1.610 ± 0.053

Table 3. Collected phonons along the [001] direction

Phonon	$Q$	$q$	Energy (THz)
LA [001] <sup>A</sup>	(2 0 5·15)	[0 0 0·15]	0·565 ± 0·017
	(2 0 5·2)	[0 0 0·2]	0·715 ± 0·021
	(2 0 5·25)	[0 0 0·25]	0·860 ± 0·020
	(2 0 5·3)	[0 0 0·3]	0·988 ± 0·015
	(2 0 5·35)	[0 0 0·35]	1·167 ± 0·020
	(2 0 5·4)	[0 0 0·4]	1·173 ± 0·032
	(0 2 5·4)	[0 0 0·4]	1·198 ± 0·030
	(0 1 4·55)	[0 0 0·45]	1·071 ± 0·028
	(0 1 4·5)	[0 0 0·5]	1·183 ± 0·026
	(0 2 5·5)	[0 0 0·5]	1·136 ± 0·039
TA [001]/[100]	(5 0 2·15)	[0 0 0·15]	0·283 ± 0·009
	(5 0 2·2)	[0 0 0·2]	0·383 ± 0·008
	(5 0 2·25)	[0 0 0·25]	0·491 ± 0·007
	(5 0 2·3)	[0 0 0·3]	0·571 ± 0·010
	(5 0 2·35)	[0 0 0·35]	0·666 ± 0·010
	(5 0 2·4)	[0 0 0·4]	0·757 ± 0·008
	(5 0 2·45)	[0 0 0·45]	0·849 ± 0·009
	(5 0 2·5)	[0 0 0·5]	0·925 ± 0·009
TA [001]/[010]	(0 4 2·15)	[0 0 0·15]	0·196 ± 0·014
	(0 4 2·2)	[0 0 0·2]	0·231 ± 0·012
	(0 4 2·25)	[0 0 0·25]	0·277 ± 0·012
	(0 4 2·3)	[0 0 0·3]	0·327 ± 0·012
	(0 4 2·35)	[0 0 0·35]	0·382 ± 0·013
	(0 4 2·4)	[0 0 0·4]	0·433 ± 0·012
	(0 4 2·45)	[0 0 0·45]	0·494 ± 0·012
	(0 4 2·5)	[0 0 0·5]	0·542 ± 0·015
Optic 1	(0 4 1·1)	[0 0 0·1]	0·896 ± 0·024
	(0 4 0·8)	[0 0 0·2]	0·840 ± 0·018
	(0 4 2·8)	[0 0 0·2]	0·849 ± 0·020
	(0 4 2·7)	[0 0 0·3]	0·768 ± 0·012
	(0 4 2·6)	[0 0 0·4]	0·665 ± 0·015
Optic 6	(0 3 1·1)	[0 0 0·1]	1·135 ± 0·037
	(0 3 0·9)	[0 0 0·1]	1·101 ± 0·044
	(0 3 1·2)	[0 0 0·2]	1·169 ± 0·022
	(0 3 0·75)	[0 0 0·25]	1·242 ± 0·030
	(0 3 1·3)	[0 0 0·3]	1·232 ± 0·029
	(0 1 4·7)	[0 0 0·3]	1·175 ± 0·029
	(2 0 5·45)	[0 0 0·45]	1·20 ± 0·1
Optic 11	(5 0 2·9)	[0 0 0·1]	1·509 ± 0·062
	(5 0 2·8)	[0 0 0·2]	1·373 ± 0·030
	(5 0 2·7)	[0 0 0·3]	1·274 ± 0·018
	(5 0 2·6)	[0 0 0·4]	1·09 ± 0·05
Optic 3	(0 0 5·1)	[0 0 0·1]	1·844 ± 0·038
	(0 0 5·2)	[0 0 0·2]	1·70 ± 0·1
	(0 2 5·3)	[0 0 0·3]	1·762 ± 0·073
	(0 2 5·4)	[0 0 0·4]	1·70 ± 0·1
	(0 2 5·5)	[0 0 0·5]	1·68 ± 0·1
Misc.	(0 3 2·1)	[0 0 0·1]	1·999 ± 0·007

<sup>A</sup> See also optic 6 for  $q = 0·35-0·5$ .

centres with an error of one scan step, i.e. 0.1 THz. No compensation was made for the effect of the instrumental resolution. The error assigned to the phonon energy was determined from either the standard deviation obtained from the fitting procedure, or one tenth of the width of the resonance, whichever was larger. The zone boundary longitudinal resonance (Fig. 1c) represents one of the poorest quality resonances measured, in terms of the counting statistics.

Table 4. Collected zone centre phonons

$Q$	Energy (THz)	$Q$	Energy (THz)
(0 4 1)	$0.921 \pm 0.025$	(0 0 5)	$1.628 \pm 0.017$
(0 3 1)	$1.167 \pm 0.044$	(0 3 2)	$1.802 \pm 0.010$
(1 4 0)	$1.144 \pm 0.027$	(0 0 5)	$1.841 \pm 0.011$

The data for the phonon branches along the orthorhombic directions are collected in Tables 1–4. These tables include the branch label, scattering vector  $Q = (hkl)$ , reduced phonon wavevector  $q = [hkl]$ , where  $h, k, l < 0.5$ , and the energy is in THz. The notation for the transverse acoustic (TA) modes indicates the propagation direction and the polarization of the atomic displacements respectively. The numbering of the optic modes indicates the order of their observation. All of the optic branches are relatively complete except for the zone centre resonance at 1.628 THz, which was very weak and could not be followed into the zone.

Table 5. Collected phonons along the [1 1 0] direction

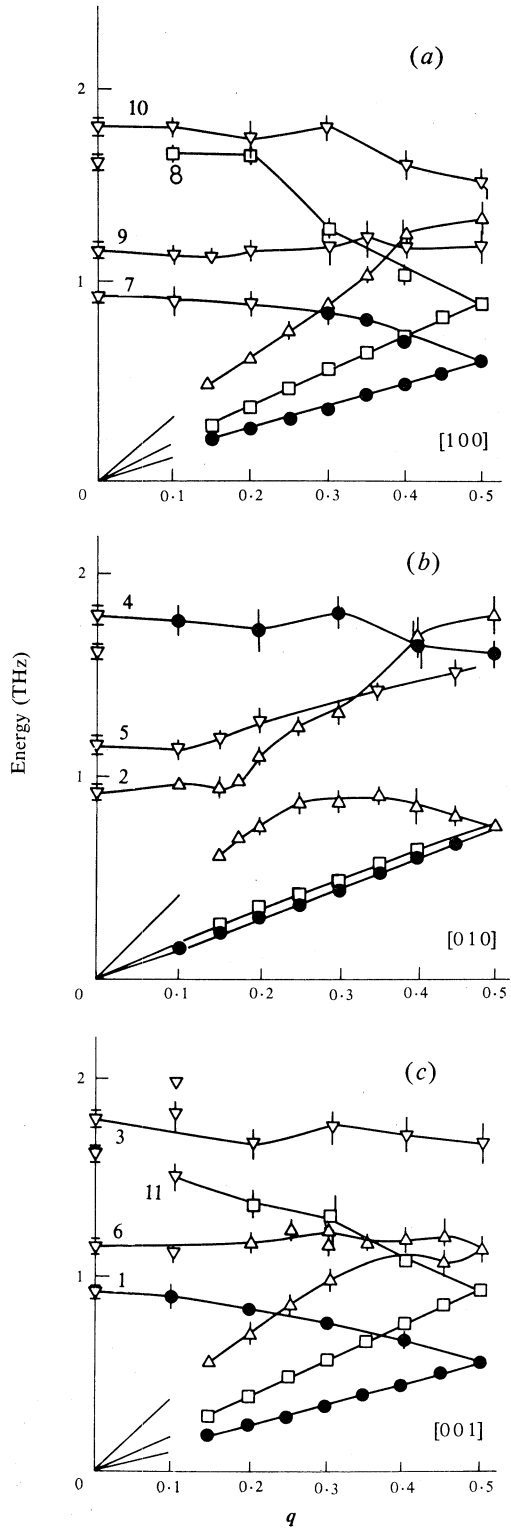
Phonon	$Q$	$q$	Energy (THz)
[1 1 0] LA	( 2.1 2.1 0)	[0.1 0.1 0]	$0.448 \pm 0.017$
[1 1 0] TA	(-2.1 3.9 0)	[0.1 0.1 0]	$0.314 \pm 0.015$

Table 6. Collected phonons along the [0 1 1] direction

Phonon	$Q$	$q$	Energy (THz)
[0 1 1] LA	(0 4.141 0.141)	[0 0.141 0.141]	$0.65 \pm 0.05$
	(0 4.212 0.212)	[0 0.212 0.212]	$0.917 \pm 0.025$
	(0 4.230 0.230)	[0 0.230 0.230]	$0.950 \pm 0.050$
	(0 4.248 0.248)	[0 0.248 0.248]	$1.00 \pm 0.05$
[0 1 1] TA	(0 4.141 0.141)	[0 0.141 0.141]	$0.458 \pm 0.010$
	(0 4.212 0.212)	[0 0.212 0.212]	$0.69 \pm 0.025$
	(0 4.248 0.248)	[0 0.248 0.248]	$0.775 \pm 0.050$
[0 1 1] Optic	(0 4.230 0.230)	[0 0.230 0.230]	$1.25 \pm 0.05$
	(0 4.248 0.248)	[0 0.248 0.248]	$1.33 \pm 0.05$
	(0 4.283 0.283)	[0 0.283 0.283]	$1.423 \pm 0.018$
	(0 4.354 0.354)	[0 0.354 0.354]	$1.60 \pm 0.05$

Tables 5 and 6 contain some phonons measured along the [1 1 0] and [0 1 1] directions respectively. The polarization of the transverse branches in both cases lies in the scattering planes and is therefore normal to [001] and [100] respectively. It proved too difficult to measure the acoustic phonons along the [101] direction, because of  $\frac{1}{2}\lambda$  contamination problems.

**Fig. 2.** Measured phonon dispersion relations below 2 THz along the principal axes together with the ultrasonically derived initial slopes. The lines are a guide to the eye only. The symbols indicate the polarizations:  $\Delta$ , longitudinal;  $\nabla$ , unknown;  $\square$ , transverse [100] in parts (b) and (c), transverse [001] in part (a);  $\bullet$ , transverse [010] in parts (a) and (c), transverse [001] in part (b).



The collected dispersion curves along the principal axes and the initial slopes of the acoustic modes, as determined from the elastic constants (Irving *et al.* 1983), are shown in Fig. 2. The measured dispersion curves along the  $[011]$  and  $[110]$  directions are presented in Fig. 3. Where an error bar is not shown in Fig. 2, the error is smaller than the symbol plotted. The lines in Fig. 2 have been drawn to serve as a guide to the probable form of the branches. The only ambiguous region of the dispersion curves, where it was difficult to determine to which branch a resonance belongs, is near the zone boundary along the  $[001]$  direction. In this region the longitudinal acoustic modes and the optic mode 6 have similar polarizations and cannot be differentiated. This ambiguity must await a theoretical model or more accurate measurements for its resolution.

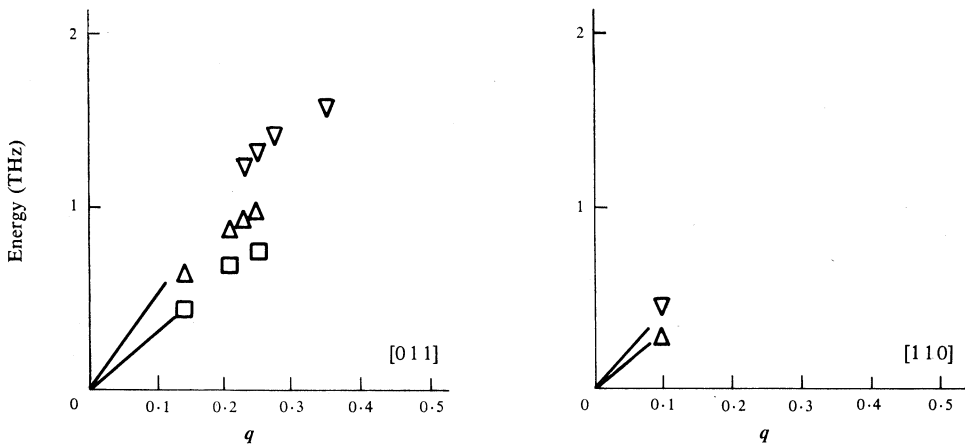


Fig. 3. Measured phonon dispersion relations below 2 THz along the  $[011]$  and  $[110]$  directions together with the ultrasonically derived initial slopes. The symbols indicate the polarizations:  $\Delta$ , longitudinal;  $\square$ , transverse; and  $\nabla$ , unknown.

In this type of study it is impossible to determine the actual atomic displacements for each phonon resonance. The form of the dynamical structure factor can only be used to determine the predominant polarization of the atomic motions from the orientation of  $\mathbf{q}$  relative to  $\mathbf{Q}$ . Where this has been possible, the assignments have been shown in Figs 2 and 3.

An interesting observation concerning the atomic displacements is a probable exchange of eigenvector between the longitudinal acoustic branch along  $[010]$ , and optic branch 2, at a wavevector of approximately  $\mathbf{q} = [00\cdot20]$ . Phonon resonances belonging to optic branch 2 were measured in reciprocal space at the points  $(04+\zeta 1)$  for  $\zeta < 0\cdot2$ . For values of  $\zeta$  approaching  $0\cdot2$ , the integrated intensity of the resonances decreased rapidly, and the branch could not be measured beyond  $\zeta = 0\cdot2$ . The branch was also found at the points  $(04+\zeta 0)$  for values of  $\zeta > 0\cdot2$ . The constant  $\mathbf{q}$  scans for  $\zeta > 0\cdot2$  also revealed the longitudinal acoustic mode resonance at a lower frequency. It is concluded that the eigenvector associated with the optic branch must be undergoing some substantial change at about  $\mathbf{q} = [00\cdot20]$  such that its behaviour is similar to the longitudinal mode. The shape of the dispersion branches in this region suggests an interchange of eigenvector at this point.

#### 4. Discussion

In general terms the overall form of the dispersion relations is similar for the  $[100]$  and  $[001]$  directions, with the  $[010]$  direction having considerably different behaviour. The unit cell is shown in Fig. 4. It can be seen that the  $[100]$  and  $[001]$  directions define the mirror planes on which all the atoms lie, while  $[010]$  is normal to the mirror planes. The symmetry of the unit cell includes screw and glide planes in the  $[100]$  and  $[001]$  directions. The space group is therefore non-symmorphic. The two-fold screw and glide operations contain sub-elements of translation symmetry which enlarge the unit cell by a factor of two (Dorner 1982). This accounts for the behaviour of the transverse acoustic modes in the  $[100]$  and  $[001]$  directions, which meet corresponding optic branches at the zone boundary. The acoustic and optic branches can be considered as a single branch using an extended zone scheme. In each case, it was found that the experimental measurements for the transverse mode extended continuously into the next Brillouin zone in reciprocal space, indicating that the behaviour of the branches was identical at the zone boundary.

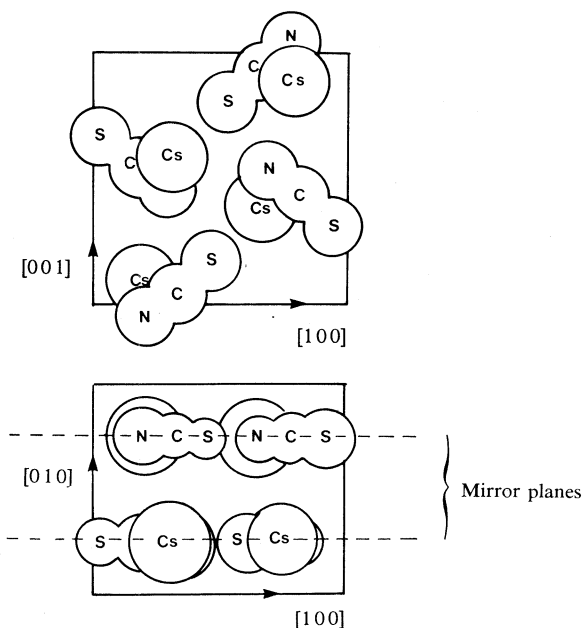


Fig. 4 Unit cell of CsSCN from Manolatos (1973).

In contrast, the behaviour of the dispersion relations along the  $[010]$  direction cannot be represented using the extended zone scheme. The longitudinal acoustic branch 'bends over' and, at the zone boundary, has a frequency close to those for the transverse polarizations. This behaviour may be merely reflecting the symmetry of the space group, in that there are neither screw nor glide planes in this direction to produce an enlarged unit cell. In simpler materials the 'bending-over' of the longitudinal modes can be associated with a second-nearest neighbour short range interaction.

The near degeneracy of the transverse acoustic modes in this direction also illustrates the tetragonal-like nature of this direction. This emphasizes the layer-like construction of the unit cell presuming similar forces within the layer and considerably different

forces between layers. This was also noted by Ti *et al.* (1977) who found the in-plane and out-of-plane bending frequencies of the thiocyanate ion to be significantly different in CsSCN.

The transverse modes in the [010] direction proved much weaker in integrated intensity compared with all the other transverse acoustic branches. While the acoustic modes in all three directions decrease in measured intensity as  $q$  increases, the branches along [010] decreased more quickly in comparison with the [100] and [001] directions. This may indicate that the atomic motions are more 'optic-like' in nature with internal vibrations within the unit cell, or that the polarization of the atomic displacements has rotated out of the scattering plane. At the zone boundary the intensities of all three acoustic modes along the [010] direction were very similar and comparable with some of the weaker optic modes measured.

On comparing our results with other experimental investigations we find that for the majority of the acoustic modes the initial slopes agree well with those derived from the elastic constants (Irving *et al.* 1983). It is also interesting to note that all the transverse branches display little dispersion, and the acoustic branches in the [110] and [011] directions have considerably higher velocities when compared with the principal directions.

Table 7. Experimental Raman peaks from Ti *et al.* (1977)

Labels	Symmetry species	Frequencies ( $\pm 0.1$ THz)	Motion type
L1, L2, L3	A <sub>g</sub>	1.14, 1.41, 2.19	'in plane'
L14, L15	B <sub>1g</sub>	1.32, 2.19	'out-of-plane'
L9, L10, L11	B <sub>2g</sub>	1.23, 1.65, 2.16	'in-plane'
L6, L7	B <sub>3g</sub>	1.38, 2.22	'out-of-plane'

Infrared and Raman spectra have been reported by Ti *et al.* (1977). While several reported Raman frequencies are less than 2 THz in energy, the lowest reported infrared frequency is 2.55 THz (85 cm<sup>-1</sup>). The Raman frequencies as taken from Ti *et al.* (1977) are listed in Table 7 along with the symmetry assignments and labels as used in the rigid-ion model (Ti *et al.* 1980a).

The variation of intensity of phonon resonances with scattering vector is given by the dynamical structure factor (DSF). In an analogous fashion to the structure factor for elastic scattering it is possible to determine the systematic absences for  $q = 0$  phonons. These conditions can be derived from the summation

$$DSF \propto \sum_k b_k \exp(\mathbf{Q} \cdot \mathbf{r}_k) \mathbf{Q} \cdot \mathbf{u}_k \exp\{-W_k(\mathbf{Q})\},$$

which relates the dynamical structure factor to atoms in the unit cell with relative coordinates  $\mathbf{r}_k$ , atomic displacements  $\mathbf{u}_k$ , scattering lengths  $b_k$  and Debye-Waller factor  $\exp\{-W_k(\mathbf{Q})\}$ . The atomic displacements for atoms occupying equivalent positions in the unit cell can be related by transformations derived from the symmetry species of the phonon. These constraints cause the summation to be zero for particular values of  $\mathbf{Q}$  independent of values for  $b_k$ ,  $W_k(\mathbf{Q})$  and the exact nature of  $\mathbf{u}_k$ .

Thus, rules for  $\mathbf{Q}$  can be formulated which must be satisfied in order that a  $q = 0$  phonon of a particular symmetry can be observed at a reciprocal lattice point. These

are summarized in Table 8. It should be noted however, that they alone are not sufficient conditions as it is possible for the atomic displacements to result in a structure factor which prevents a particular phonon from being observed at a specific reciprocal lattice point. However, phonons of a particular symmetry cannot be observed in violation of these conditions.

**Table 8. Conditions for elastic and  $q = 0$  inelastic scattering for  $Pnma$**

Symmetry species	Type of reciprocal lattice point		
	$(hk0)$	$(h0l)$	$(0kl)$
Elastic	$h$ even	No conditions	$k+l$ even
$A_g$	$h$ even, $h \neq 0$	$h$ or $l \neq 0$	$k+l$ even, $l \neq 0$
$A_u$	$h$ odd, $k \neq 0$	Never	$k+l$ odd, $k \neq 0$
$B_{3g}$	$h$ odd, $k \neq 0$	Never	$k+l$ even, $k \neq 0$
$B_{3u}$	$h$ even, $h \neq 0$	$h$ or $l \neq 0$	$k+l$ odd, $l \neq 0$
$B_{1g}$	$h$ even, $k \neq 0$	Never	$k+l$ odd, $k \neq 0$
$B_{1u}$	$h$ odd, $h \neq 0$	$h$ or $l \neq 0$	$k+l$ even, $l \neq 0$
$B_{2g}$	$h$ odd, $h \neq 0$	$h$ or $l \neq 0$	$k+l$ odd, $l \neq 0$
$B_{2u}$	$h$ even, $k \neq 0$	Never	$k+l$ even, $k \neq 0$

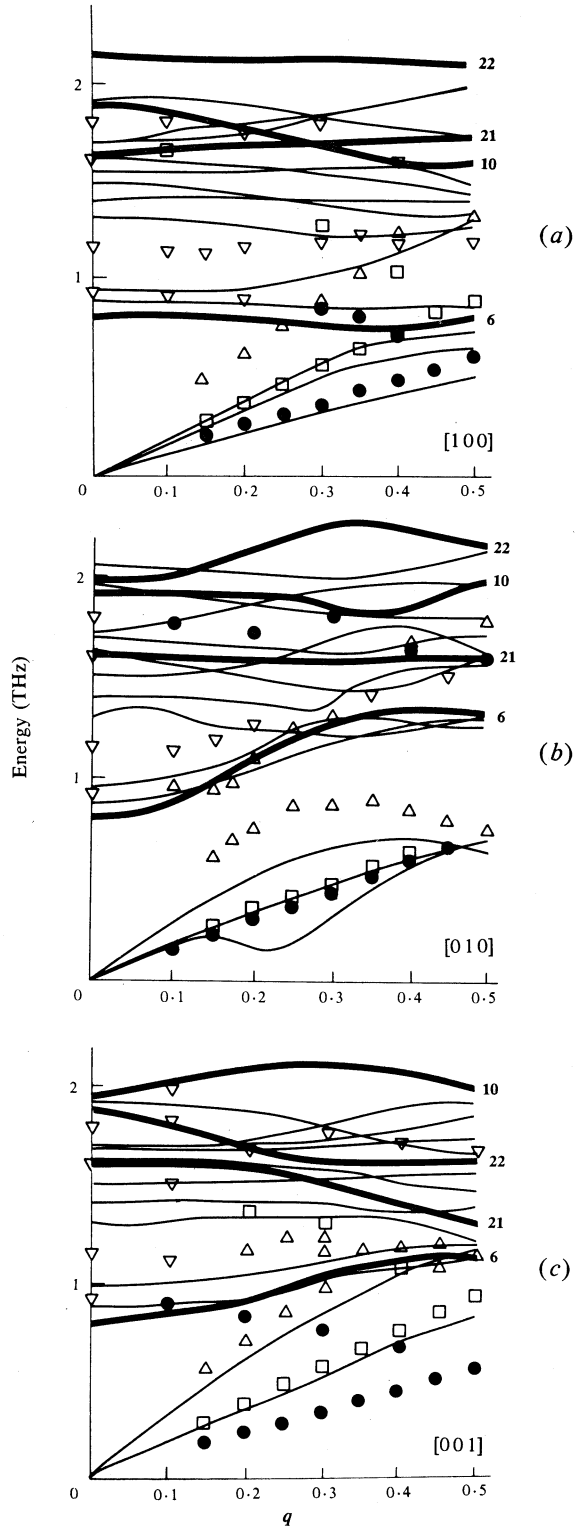
**Table 9. Zone centre symmetries**

Energy (THz)	Symmetry	Label	Spectroscopy
$0.921 \pm 0.08$	$A_u$	L17	—
$1.144 \pm 0.09$	$B_{3g}$	L6	$1.32 \pm 0.1$
$1.167 \pm 0.12$			
$1.628 \pm 0.05$	$B_{2g}$	L10	$1.65 \pm 0.1$
$1.802 \pm 0.03$	$B_{3u}$	L22 (or L21)	—
$1.841 \pm 0.03$			

The probable symmetries of the measured zone centre phonons derived from the above conditions, together with the labels used by Ti and Ra in their model, are presented in Table 9. The uncertainty in the energy has been taken as three times the standard deviation from the fitting procedure. The only assumptions made in these symmetry assignments were: that where the measured frequency could not be related to a Raman active mode, it had an infrared active symmetry; that the resonance with  $A_u$  symmetry is the lowest mode of this symmetry; and that the resonance with  $B_{3u}$  symmetry is either L22 or L21. It can be seen that there is agreement, within the combined experimental uncertainties, with the Raman frequencies.

However, there is a serious discrepancy between the neutron results and the Raman spectra in that the other four zone centre Raman frequencies below 2 THz (L1, L2, L14, L9) were not observed. We cannot state emphatically that no modes other than those reported here exist below 2 THz as it is possible that the resolution and 'focusing' restrictions of the instrument, along with the form of the dynamic structure factor, prohibit these modes from being observed within the limited region of reciprocal space accessible. However, from the exhaustive nature of the present search we believe that if such modes exist they are considerably less intense than those reported here.

**Fig. 5.** Rigid-ion model calculations of Ti and Ra (1980*b*) superimposed over the measured dispersion curves. The branches corresponding to the assigned symmetries for the measured optic resonances have been emphasized for clarity. The numbering corresponds to that of Ti and Ra.



The comparison between the rigid-ion model of Ti and Ra (1980*b*) and the experimental dispersion curves (see Fig. 2) is shown in Fig. 5. There are considerable discrepancies between the two, even with allowance for the absence of some of the modes from the experimental results. This can be expected as no attempt has been made to modify the potential parameters in the light of the new information obtained from the elastic constants and the measured dispersion curves. Ti and Ra generated their results from potential parameters derived solely from lattice stability criteria.

In general the calculated acoustic branches do not compare well with the experimental results. The best correspondence occurs in the [0 1 0] direction for one of the transverse modes. However, the other transverse branch has a pronounced dip which is not seen in the measured curves. One transverse mode in the [0 0 1] direction has imaginary frequencies and was not displayed by Ti and Ra. A more serious discrepancy is that at the zone boundary the acoustic modes do not connect with optic modes in the [1 0 0] and [0 0 1] directions.

Comparison with the optic branches is complicated by the multitude of calculated branches. Consequently, we restrict our comments to those branches that have symmetries which correspond to those assigned to the zone centre modes (Table 9). The L17 branch is not shown because it has imaginary frequencies across the zone. In broad terms, the model best fits the dispersion relations along the [0 1 0] direction. It mirrors the correct behaviour of the longitudinal mode and the gap between the measured optic and acoustic modes. The correspondence in the other two directions is more difficult to find. As noted above, the model was found (Ra *et al.* 1978) to be in reasonable agreement with the available optical spectra, with the poorest agreement occurring for some low energy modes. The measured dispersion behaviour indicates that the model is most accurate in the region of the zone centre which may suggest that the underlying assumptions and interatomic potentials are more realistic in this region.

**Table 10. Comparison of experimental and theoretical zone centre energies**

Zone centre energy (THz)	$Q$	Label	Theoretical energy (THz)	$I_Q/I_{Q_{\max}}$	$Q_{\max}$
0.92	(0 4 1)	L17	Imaginary	1.0	(0 4 1)
1.14	(0 3 1)	L6	0.73	0.6	(0 5 1)
1.17	(1 4 0)			1.0	(1 4 0)
1.63	(0 0 5)	L10	1.92	0.66	(0 1 4)
1.80	(0 3 2)	L21	1.75	0.001	(0 2 3)
		L22	1.89	0.27	(0 0 5)
1.84	(0 0 5)	L21	1.75	0.85	(0 2 3)
		L22	1.89	1.0	(0 0 5)

If we restrict ourselves to  $q = 0$ , the theoretical energies may be compared with the zone centre measurements as in Table 10. Predicted values for  $I_Q$ , the intensity for a particular phonon mode measured at the position  $Q$ , relative to  $I_{Q_{\max}}$ , the maximum intensity at the position  $Q_{\max}$ , have been calculated, assuming a constant Debye-Waller factor, from the dynamical structure factors for all reciprocal lattice points in the region of reciprocal space accessible to the instrument. Values for  $I_Q/I_{Q_{\max}}$  and  $Q_{\max}$  are also given in Table 10.

Although the calculated zone centre energies do not agree with the measured energies, the predicted values for  $I_Q$  are all significantly large at the points in reciprocal space where the resonances were detected. This may indicate that, although the model eigenvalues are inaccurate, the form of the eigenvectors is generally correct. It should be noted, however, that the model uses a reduced dynamical matrix with symmetry coordinates. This forces the components of the eigenvectors to have the symmetry corresponding to their symmetry representation. Furthermore the tabulation of dynamical structure factors would indicate that there are several reciprocal lattice points with similar numerical values for  $I_Q$ . Thus, the observation of a resonance at a specific point with a large predicted value for  $I_Q$  has less relevance when the failure to detect resonances at several other points, calculated to be equivalent, is taken into account. However, the important effect of instrumental resolution was not considered in these calculations, and its effect would be to impose additional constraints on the position for maximum intensity.

One valuable result from these calculations is the resolution between the assignment of the modes L21 and L22 to the zone centre resonances at 1.80 and 1.84 THz. We believe that both resonances probably represent the same phonon. The relative intensities calculated from the structure factors suggest that this phonon corresponds to L22 rather than L21.

Perhaps the greatest deficiency of the rigid-ion model is the neglect of ionic polarizability. Ti and Ra were forced to make this simplification because a lack of experimental measurements limited the size of their parameter set. In comparison with other ionic solids, such as the alkali halides and cyanides, successful models have required first and second neighbour short range interactions within a shell model formulation. The models developed for the cyanides are of particular relevance because of their treatment of a linear anion (Jex and Maetz 1978). These 'rigid-shell' models indicate the necessity to treat the ionic polarizability of the anion in terms of a rigid-shell and rigid-core configuration. The formulation allows librational-translation coupling and dipolar interactions between anions to be included (Luty and Pawley 1974).

The alkali cyanides represent a group of solids, closely similar to the alkali thiocyanates, for which phonon dispersion curves have been measured. These materials also consist of linear anions with similar order-disorder phase transitions. Unfortunately, direct comparison with these room temperature dispersion curves is not possible because they correspond to the cubic disordered phase. In the case of KCN, the single-phonon resonances were difficult to measure at room temperature because of the large vibrational amplitudes of the anions, and a large multi-phonon background (Rowe *et al.* 1975). The most interesting result was an anomalous softening of the transverse acoustic modes at the zone centre which was related to the translational-libron coupling. In contrast, caesium thiocyanate at room temperature does not show any softening of the transverse acoustic modes. This suggests that such a coupling, if it exists, is weak at this temperature.

## 5. Conclusions

The present investigation represents the first step towards a more realistic potential model for the thiocyanates. While it does not provide a complete description of the lattice modes of caesium thiocyanate, as the behaviour of many branches is yet to be

determined, this investigation has highlighted the shortcomings of the rigid-ion model of Ti and Ra. The model only offers a limited description of the experimental data and its successes appear to be largely due to symmetry constraints.

Further work nearer the transition temperature is required to understand the lattice dynamics associated with rotational order-disorder type phase transitions and the problems of librational-acoustic coupling

### Acknowledgments

This work could not have been undertaken without an Australian Institute of Nuclear Science and Engineering studentship (M.A.I.) and the support of the Australian Research Grants Scheme. Equipment was made available by the Australian Atomic Energy Commission. We acknowledge the many useful discussions held with Dr S. S. Ti.

### References

- Dorner, B. (1982). 'Coherent Inelastic Neutron Scattering in Lattice Dynamics', p. 23 (Springer: Berlin).
- Irving, M. A., Prawer, S., Smith, T. F., and Finlayson, T. R. (1983). *Aust. J. Phys.* **36**, 85.
- Jex, H., and Maetz, C. J. (1978). *Phys. Status Solidi (b)* **85**, 511.
- Klement, W., Jr (1976). *Bull. Chem. Soc. Jpn* **49**, 2148.
- Luty, T., and Pawley, G. S. (1974). *Phys. Status Solidi (b)* **66**, 309.
- Manolatos, S., Tillinger, M., and Post, B. (1973). *J. Solid State Chem.* **7**, 31.
- Ra, O., Ti, S. S., and Kettle, S. F. A. (1978). *J. Chem. Phys.* **68**, 2638.
- Rowe, J. M., Rush, J. J., Vagelatos, N., Price, D. L., Hink, D. G., and Susman, S. (1975). *J. Chem. Phys.* **62**, 4551.
- Ti, S. S., Kettle, S. F. A., and Ra, O. (1977). *Spectrochim. Acta A* **33**, 111.
- Ti, S. S., and Ra, O. (1980a). *J. Chem. Phys.* **73**, 5738.
- Ti, S. S., and Ra, O. (1980b). *J. Chem. Phys.* **73**, 5749.

Manuscript received 16 January, accepted 27 March 1984

